ORIGINAL ARTICLE

Study on the influence of vibration parameters in the twin-roll strip vibration cast-rolling process

Minghan Sun[1,2] · Zhiwang Zhu[1,2] · Likang Zheng[1,2] · Shipeng Guo[1,2] · Fengshan Du[1,2]

Abstract

In this paper, the influence of vibration parameters on twin-roll strip vibration cast-rolling is studied. Through a comparison of vibration and nonvibration cast-rolling experiments with a 7075 aluminum alloy, it is found that the mechanical vibration introduced during the cast-rolling process can refine the grains and inhibit segregation. A thermal-flow-coupled numerical simulation model of the actual twin-roll strip vibration cast-rolling process is constructed to study the time-domain characteristics and frequency-domain characteristics of the flow field and temperature field in the molten pool, and the model is verified by experiments. The simulation results show that the disturbing effect of vibrations on the flow field in the molten pool can increase the nucleation rate by promoting dendrite fusing and inhibit the segregation of alloying elements. The vibration also affects the temperature field. During vibration cast-rolling, the height of the kiss point changes sinusoidally with time. Based on an analysis of the influence of the amplitude and vibration frequency on the temperature field and flow field, the optimal vibration parameters of the vibration cast-rolling process are determined and provide a foundation for the promotion and application of the new technology of vibration cast-rolling.

Keywords Vibration · Cast-rolling · Vibration parameters · Molen pool · Flow field · Temperature field

1 Introduction

The twin-roll strip cast-rolling process effectively combines continuous casting and rolling into one process and can directly fabricate a thin strip from molten metal, thereby having the advantages of a short processing time, low cost, and low energy consumption. Therefore, it is currently one of the most attractive forming technologies in the metallurgical industry [1–3]. Cast-rolling involves a sub-rapid cooling solidification process, so the fault tolerance of the process is poor, and the precise matching of many process parameters, such as the rolling speed, liquid level, casting temperature, roll diameter, and roll gap width, is required. Therefore, it is necessary to explore the influence of these parameters on the flow field and temperature field in the molten pool. However, since the twin-roll strip cast-rolling process is dynamic and rapid and the temperature is high, it is difficult to observe the conditions in the molten pool in real time during an experiment. The comprehensive modeling of the fluid flow, heat transfer, and solidification processes during cast-rolling is indispensable [4, 5].

Zhang et al. [6] constructed a mathematical model using fluid dynamics to study the effect of the metal delivery system on the fluctuation of the molten pool. Miao et al. [7] established a three-dimensional model of fluid flow and heat transfer in a twin-roll continuous casting process by the finite element method and studied the effects of different parameters on the fluid flow and temperature field. The simulation results were verified by experiments. Bae et al. [8] carried out a numerical study on the flow and heat transfer characteristics in the molten pool at rolling speeds of 4–9 rpm to determine the optimal process for twin-roll thin strip cast-rolling. Zhang et al. [9, 10] studied the variation of the temperature field and solidification end point in the molten pool under different roll gap widths and roll diameters. Rodrigues et al. [4] used the two-phase Eulerian–Eulerian volume-averaging model to analyze the viscoplastic flow of semisolid metal melts. It was

✉ Fengshan Du
fsdu@ysu.edu.cn

1 National Engineering Research Center for Equipment and Technology of Cold Strip Rolling, Yanshan University, Qinhuangdao 066004, Hebei, China

2 College of Mechanical Engineering, Yanshan University, Qinhuangdao 066004, Hebei, China

Fig. 1 Schematic diagram of twin-roll strip vibration cast-rolling process
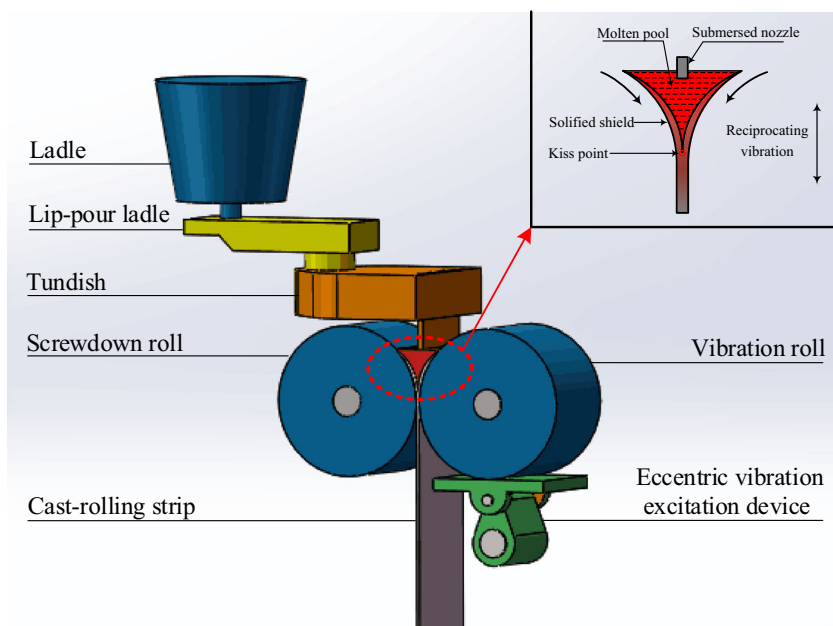
found that the macrosegregation during the casting process was intrinsically linked to the mushy zone deformation forced by the plastic deformation stage.

In the traditional cast-rolling process, the rolls are usually fixed, the flow field is relatively stable, and central segregation is very likely to occur [11, 12]. For the temperature field, there is a single direction temperature gradient across the roll surface. The grains in the cast-rolled strip are generally coarse columnar crystals, which have poor mechanical properties and a high tendency to crack when subjected to high-temperature plastic deformation [13]. To solve this problem, Du et al. [14–16] proposed the theory of vibration cast-rolling, in which one of the two cast-rolling rolls vibrates vertically under an external force (as shown in Fig. 1). In the molten pool, the

nucleation rate is enhanced by the mechanical vibration of the rolls, and the tendency to enrich the material with alloying elements is suppressed. At the same time, during the plastic deformation stage, the bidirectional shear force applied by the vibration to the metal in the rolling zone promotes dynamic recrystallization. In this way, the mechanical properties of the cast-rolled strip can be effectively upgraded to enable the commercialization of twin-roll strip cast-rolling in the steel industry.

Wei et al. [16] revealed the microstructure evolution mechanism during the vibration cast-rolling process but did not analyze the influence of the vibration on the flow field and temperature field in the molten pool. Research by others did not reveal the time-domain characteristics of the influence of vibration on the flow field and temperature field of the molten pool, and the accuracy of the simulation model was not reasonably verified as well [14, 15]. In view of this, a numerical simulation model of the vibration casting-rolling process that connects the fluid flow, heat transfer, and solidification processes is established in this paper; also, the variation of the flow field and temperature field in the molten pool under vibration are described in detail, and the temperature data at the exit of the strip are collected to verify the accuracy of the model.

Fig. 2 The $\varphi 500 \times 350$ mm twin-roll strip micro-vibration cast-rolling mill used herein

Table 1 Chemical composition of 7075 aluminum alloy (%, mass fraction)

Mg	Zn	Cu	Mn	Cr	Si	Fe	Ti	Al
2.72	5.62	1.64	0.30	0.24	0.40	0.50	0.20	The remaining

Table 2 Tensile test results of the cast-rolling strips

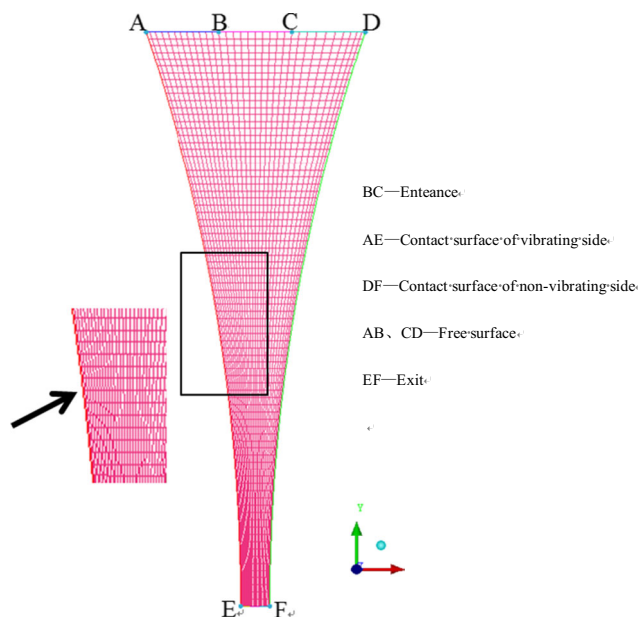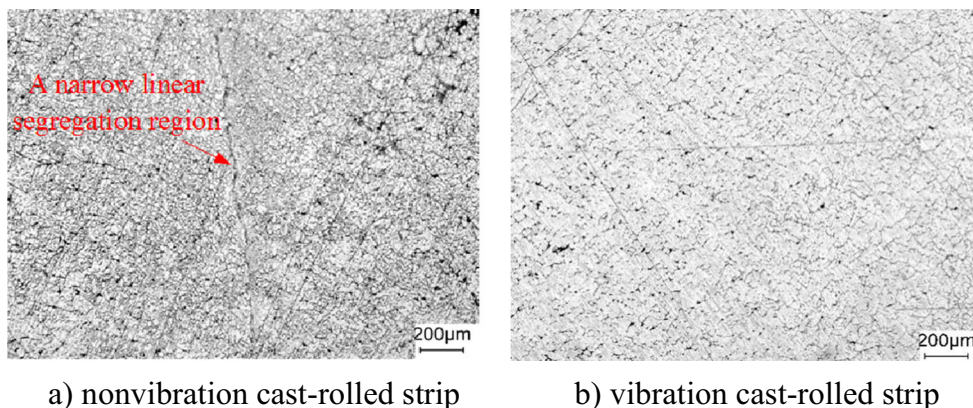|	650 °C, nonvibration	650 °C, vibration
Tensile strength/MPa	209.2	237.5
Yield strength/Mpa	51.2	56.3
Elongation/%	6.9	8.6

2 Experimental methods

The cast-rolling experiments were carried out on a φ500 × 350 mm twin-roll strip micro-vibration cast-rolling mill at Yanshan University (as shown in Fig. 2). A 7075 aluminum alloy was used as the experimental object, and its composition is listed in Table 1. The experimental conditions were as follows: the casting temperature was 650 °C, the roll gap width was 4 mm, the cast-rolling speed was 5 m/min, the cooling water pressure was 0.6 MPa, and the height of the molten pool was 80 mm. An experiment that compares vibration and nonvibration cast-rolling was carried out, and the vibration frequency was 25 Hz and the amplitude was 0.38 mm.

The temperature of the strip at the rolling exit was monitored in real time using an infrared detector to obtain temperature variation data throughout the experiment. After the experiment, tensile tests of the cast-rolled strips were carried out by using a CSS-44100 electronic experimental machine according to the GB/T 228-2002 experimental standard. The tensile direction was along the rolling direction. There were 3 samples in each group, and the average was taken as the final result. In addition, the microstructure of the strips was observed using a Leica DMI 5000M metallographic microscope. The tensile specimens and the metallographic specimens were cut from the center of the strip.

The tensile test results are shown in Table 2. The yield strength, tensile strength, and elongation of the vibrating cast slab increased by 9.22%, 14.95%, and 31.25%, respectively, compared with those of the nonvibration slab, indicating that the vibration effectively improved the comprehensive mechanical properties of the cast-rolled strip.

BC—Enteance

AE—Contact surface of vibrating side

DF—Contact surface of non-vibrating side

AB、CD—Free surface

EF—Exit

Fig. 4 Geometric model of the thermal-flow-coupled numerical simulation

Figure 3 shows the microstructure of the vibration cast-rolled strip and nonvibration cast-rolled strip. As seen from the figure, the crystal grains in the nonvibration cast-rolled strip were coarse, and a narrow linear segregation region appeared in the core of the strip. In contrast, the segregation phenomenon in the vibration cast-rolled strip was significantly suppressed, there was no obvious segregation region, but only a small amount of point-like segregation defects, and the grains decreased in size, indicating that vibration can effectively improve the microstructure of cast-rolled strips.

3 Theoretical research

The twin-roll strip cast-rolling process is a complex process involving multiple phenomena, such as molten metal flow, solidification, and dendrite growth. It is necessary to establish a multifield coupled math empirical model to analyze the

Fig. 3 Microstructure of the vibration and nonvibration cast-rolled strips. **a** Nonvibration cast-rolled strip. **b** Vibration cast-rolled strip

A narrow linear segregation region

200μm

a) nonvibration cast-rolled strip

200μm

b) vibration cast-rolled strip

Table 3 Simulation condition

Parameter	Value	Parameter	Value
Roll diameter (mm)	500	Ambient temperature (K)	300
Cast-rolling speed (m/min)	5	Environmental pressure (Pa)	101,325
Roll gap width (mm)	4	Latent heat (KJ/Kg)	352
Density (kg/m^3)	2760	Liquidus temperature (K)	903
Viscosity (kg/m s)	0.0014	Molten pool height (mm)	80
Solidus temperature (K)	793	Casting temperature (K)	923

distribution trends for the flow field and temperature field in the molten pool.

3.1 Governing equation

During the twin-roll strip cast-rolling process, the molten metal flows rapidly in the molten pool. The use of a laminar flow model reduces the effect of the liquid flow on the temperature distribution, so the k-ε turbulence model is chosen for calculation. Its governing equation is as follows:

$$\frac{\partial}{\partial t}(\rho\varphi) + \frac{\partial}{\partial x_k}(\rho u_k \varphi) = \frac{\partial}{\partial x_k}\left(T_\varphi \frac{\partial \varphi}{\partial x_k}\right) + S_\varphi \tag{1}$$

where $\varnothing$ is the transmission variate, $T_\varnothing$ is the equivalent heat conduction, and $S_\varnothing$ is the source term for the momentum or energy equation.

3.2 Low Reynolds number model

The fluid in the molten pool during the twin-roll strip cast-rolling process is mainly turbulent. Nevertheless, due to the constant change in the boundary between the molten pool and the rolls during the vibration cast-rolling process, if the standard turbulence model is used, the wall function cannot be accurately determined. In contrast, a low Reynolds number turbulence model does not require a wall function, so it is easy to handle the turbulence characteristics of fluids, two-phase regions, and walls. Therefore, the low Reynolds number

turbulence model proposed by Lam and Brehorst is used to solve the problem.

3.3 Metal flow in the liquid-solid two-phase region

When the temperature of the metal is between the solidus and the liquidus, the dendritic framework in the mushy zone can be equivalent to that in a porous medium by the enthalpy-porosity method, and the liquid metal flows in the pores of the porous medium, the momentum of which satisfies the formula:

$$S' = S - \frac{(1-\beta)^2}{\beta^3} A_{mush}(v - v_p) \tag{2}$$

where S is the momentum value of the fluid in the molten state; β is the liquid fraction of the region; v and v_p are the speed of the liquid phase and solid phase, respectively; and A_{mush} is a mushy zone constant, which is related to the secondary dendrite spacing λ of the solidified structure according to the report by BANKI R et al. (2008). The Kirkwood model shows that the secondary dendrite spacing is related to the cooling rate: $\lambda = A(T)^{-n}$. Therefore, the expression of the two-phase zone (i.e., the mushy zone) constant A_{mush} is as follows:

$$A_{mush} = \frac{180\mu}{\lambda^2} = \frac{180\mu}{\left(A(\overline{T})^{-n}\right)^2} \tag{3}$$

where μ is the viscosity of the metal fluid, A and n are solidification constants of the aluminum alloys, and $\overline{T}$ is the average cooling rate.

Table 4 Thermophysical parameters of 7075 aluminum alloy

Temperature (K)	20	100	200	300	400	450	470	500	550	600	650
Heat conductivity coefficient (W·m^{-1}·K^{-1})	163	174	125	190	180	77		70		80	
Heat transfer coefficient (W·m^{-1}·K^{-1})	1500		2500	11,000				10,000			
Specific heat (J·kg^{-1}·K^{-1})	1000		1090	1150	1220			3140	1000		

Fig. 5 Comparison of the experimental and simulated results of the strip temperature at the rolling exit during vibration and nonvibration cast-rolling. **a** Nonvibration cast-rolling. **b** Vibration cast-rolling

a) nonvibration cast-rolling

b) vibration cast-rolling
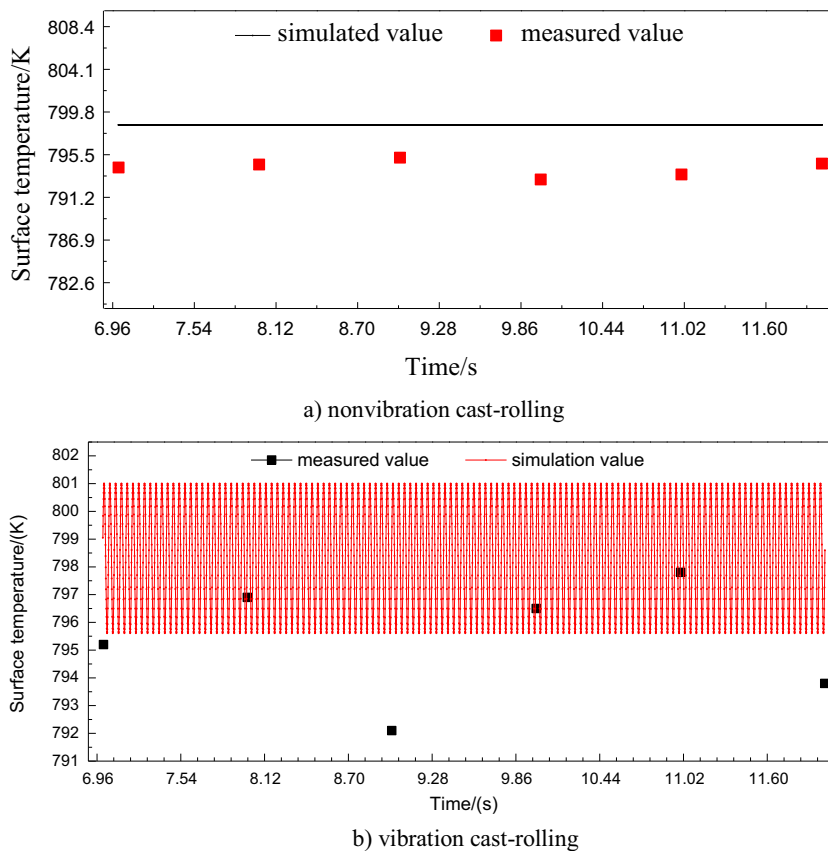
3.4 Energy equation for solidification

The solidification process of the molten metal satisfies the energy balance formula:

$$\frac{\partial}{\partial t}(\rho H) + \nabla \cdot (\rho v H) = \nabla \cdot (k \nabla T) + S_n \tag{4}$$

where ρ is the density of the material; H is the enthalpy during solidification that includes two parts: the sensible and latent heats; S_n is the energy exchange between the unit body and the environment; and ∇ is a Hamiltonian differential operator, whose expression is as follows:

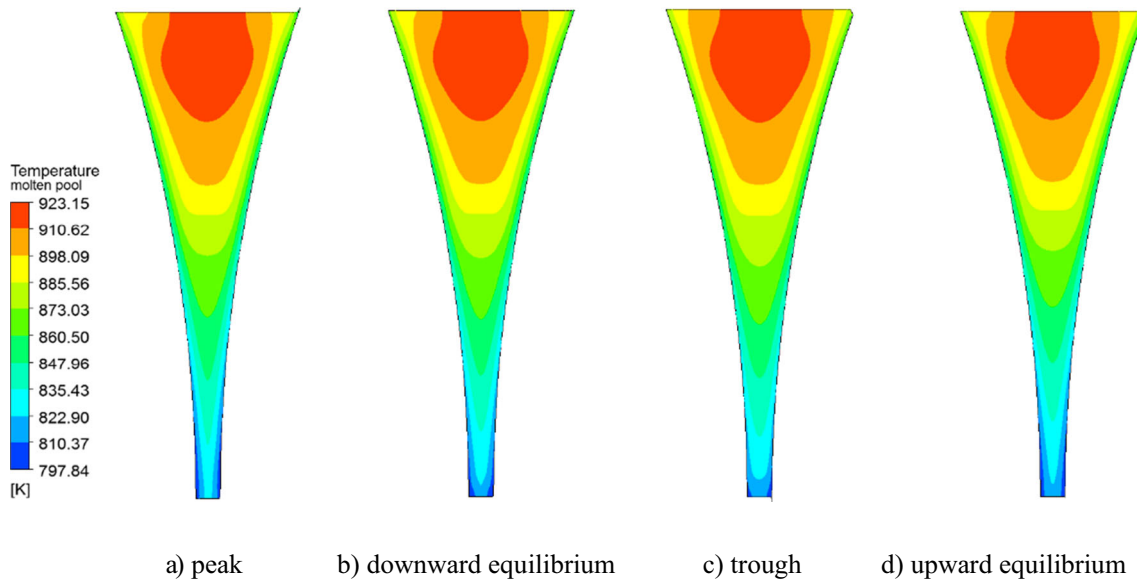$$\nabla = i\frac{\partial}{\partial x} + j\frac{\partial}{\partial y} + k\frac{\partial}{\partial z} \tag{5}$$

3.5 Dynamic mesh model

During vibration cast-rolling, the boundary between the molten pool and the vibrating roll is in motion, so a dynamic mesh model is used to solve the problem. The conservation equation is as follows:

$$\frac{\partial(\rho\phi)}{\partial t} + \nabla \cdot \left[\rho\phi\left(\vec{u} - \vec{u}_g\right)\right] = \nabla \cdot (\Gamma\nabla\phi) + S \tag{6}$$

Table 5 Different vibration parameters for the simulation experiments

Number	Amplitude (mm)	Vibration Frequency (Hz)	Number	Amplitude (mm)	Vibration frequency (Hz)
1	0.20	10	7	0.20	10
2	0.38	10	8	0.20	15
3	0.56	10	9	0.20	20
4	0.83	10	10	0.20	25
5	1.00	10	11	0	0
6	0.20	5			

a) peak   b) downward equilibrium   c) trough   d) upward equilibrium

Fig. 6 Temperature field in the molten pool at different vibration phases when the vibration frequency is 10 Hz and the amplitude is 0.38 mm. **a** Peak, **b** downward equilibrium, **c** trough, and **d** upward equilibrium

where ρ is the density (kg/m3), $\vec{u}$ is the velocity vector of the fluid (m/s), Γ, is the diffusion coefficient, and S_y is the source item.

4 Mathematical model

Based on the above fluid dynamics and solidification theory, a thermal-flow-coupled numerical simulation model of the molten pool was constructed by using Fluent software to analyze the influence of the vibration parameters on the flow field and temperature field in the molten pool.

4.1 Assumptions

The mathematical model herein was based on the following assumptions:

1. The actual three-dimensional structure was reduced to a two-dimensional model, as the flow field and temperature field in the molten pool are evenly distributed along the width direction of the roll.
2. The molten metal in the molten pool is a kind of incompressible Newtonian fluid.
3. Hot deformation of the rolls and strips can be ignored.
4. No slippage occurs on the surface of the strip and the rolls.
5. The thermal conductivity and viscosity of the metal are functions of the temperature.
6. The physical parameters of the rolls are constant.
7. Fluctuations of the molten pool level can be ignored. Aboutalebi found that the turbulent energy of the molten pool level is extremely small due to the high surface tension of the molten metal due to the thermal-flow-coupled model of continuous casting.
8. The solidified shell grows in the form of columnar crystals in the <001> direction opposite to the heat transfer direction, regardless of the presence of a gap.

Fig. 7 The history of the temperature at the midpoint of the rolling exit under different vibration frequencies when the amplitude is 0.2 mm
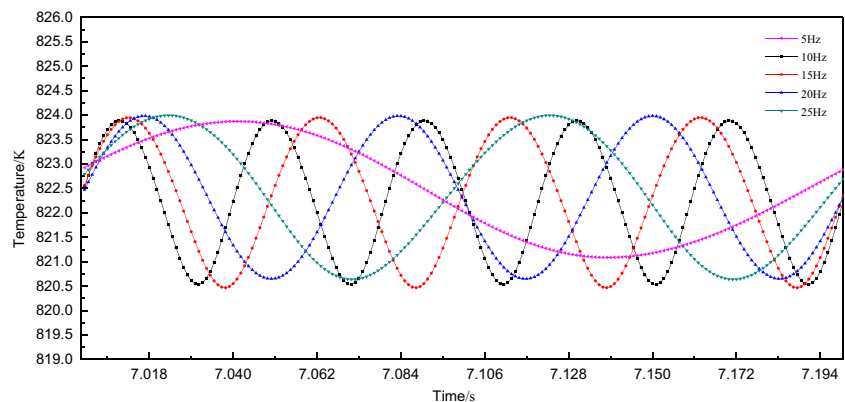
Fig. 8 The history of the temperature at the midpoint of the rolling exit under different amplitudes when the vibration frequency is 10 Hz
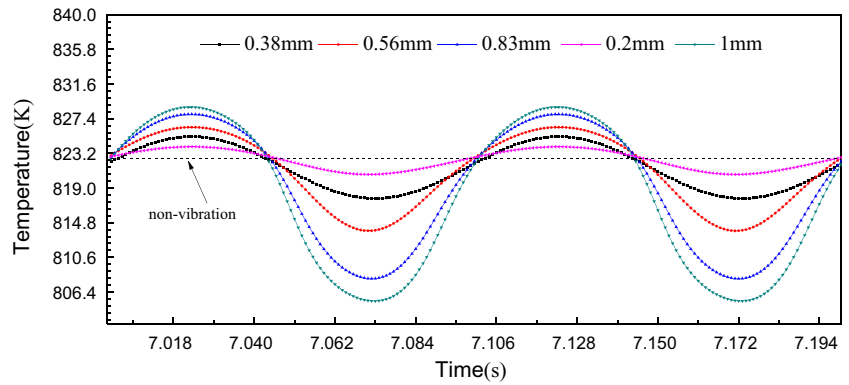
9. The latent heat of the solid-phase transformation can be neglected as it is much smaller than the latent heat of solidification.

4.2 Boundary conditions

The geometric model of the molten pool was established according to the actual situation, as shown in Fig. 4. The height of the molten pool is 80 mm. To maintain this height, the inlet flow of the metal should be consistent with the outlet.

The inlet boundary condition (BC) is as follows:

$$T_{in} = T_c, v_{in} = \frac{v \cdot B \cdot \rho_s}{C \cdot \rho_l}, k_{in} = \frac{3}{2}(v_{in}I)^2, \text{and } \varepsilon_{in} = \frac{k_{in}^{1.5}}{0.3D_h} \quad (7)$$

where T_c is the casting temperature (°C), v is the cast-rolling speed (mm/s), I is the turbulence intensity, B is the roll gap width (mm), ρ_s is the solid-phase density (kg/m³), ρ_l is liquid-phase density (kg/m³), k_{in} is the inlet tubulence energy (kw), ε_{in} is the dissipation rate of the inlet turbulent energy, and D_h is the hydraulic diameter of the feeding system (m).

The outlet boundary condition (EF) is as follows:

$$v_{out} = v \quad (8)$$

where v_{out} is the outlet flow rate.

Based on the assumption that the wall has no slip, the boundary conditions of the nonvibrating side roll surface can be described as follows:

$$\overline{v_x} = v \cdot \cos\beta, \overline{v_y} = v \cdot \sin\beta, \text{and} -\lambda_{eff} \cdot \frac{\partial T}{\partial n} = h_{left}(T - T_{roller}) \quad (9)$$

where h_{left} is the convective heat transfer coefficient of the left roll surface (W/m² K), T is the temperature of the molten pool (K), T_{roller} is the temperature of the roll surface (K), and β is the contact angle between the boundary element and the roll surface.

The boundary condition of the vibration-side roll surface is as follows:

$$\overline{v_x} = v \cdot \cos\beta, \overline{v_y} = v \cdot \sin\beta \quad (10)$$

The vibration displacement equation is as follows:

$$f(t) = A\sin(2\pi f \cdot t) \quad (11)$$

where A is the amplitude (mm), f is the vibration frequency (Hz), and t is the time (s).

The convective heat transfer coefficient comprehensively considers the contact thermal resistance, the equivalent thermal radiation, and the thickness of the air gap between the vibration-side roll and the molten pool. Therefore, the convective heat transfer coefficients on the two sides of the molten

Fig. 9 The history of the kiss point height under different vibration frequencies when the amplitude is 0.2 mm
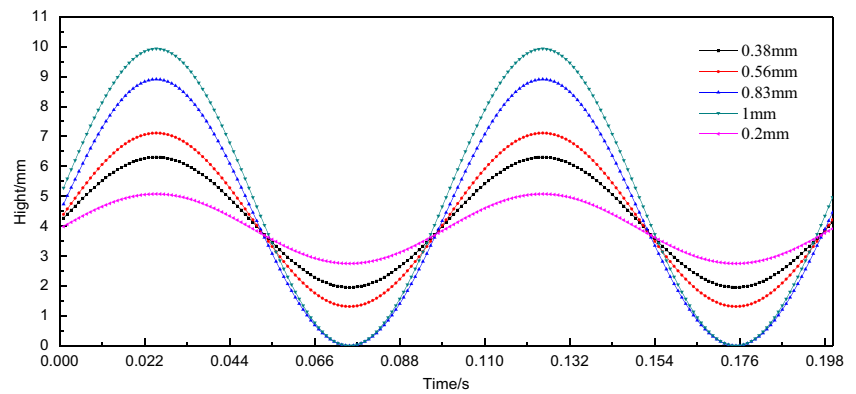
pool are not the same, but they are all in the range from 4000
to 6000 W/(m² K).

The parameters required for the mathematical model are
shown in Table 3, and the thermophysical properties of the
7075 aluminum alloy are shown in Table 4.

Temperature data at several time points were collected dur-
ing the simulation and compared with the temperature collect-
ed during the experiment (as shown in Fig. 5). It can be seen
from the figure that the experimental values and the simulated
values are basically consistent, but the experimental values are
approximately 3–5 K smaller than the simulated values. This
is because the scale that formed on the surface of the high-
temperature strip affects the heat radiation rate, thereby reduc-
ing the accuracy of the infrared detector. Through the above
comparison, the rationality of the simulation model is verified.

5 Analysis and discussion

To describe the temperature field and flow field in the molten
pool during vibration cast-rolling in detail and study the influ-
ence of vibration parameters on them, a series of simulations
was carried out under different vibration parameters (as shown
in Table 5).

5.1 Effect of the vibration on the temperature field

5.1.1 Time-domain characteristics of the temperature field

The simulation results show that the temperature field in the
molten pool has obvious time-domain characteristics under
vibration. It can be seen from Fig. 6 that when the rolls are
in different vibration phases, the temperature distribution in
the molten pool is basically the same. However, there are
certain differences in the specific values, which indicates that
the flow field change caused by vibration can affect the heat
exchange state of the roller surface on the vibration side and
the nonvibration side at the same time, thereby maintaining a
relatively uniform temperature distribution in the molten
pool.

To explore the influence of the vibration parameters on the
temperature field in the molten pool, the variation histories of
the temperature at the center of the rolling exit during vibra-
tion cast-rolling with different amplitudes and vibration fre-
quencies were simulated (as shown in Figs. 7 and 8). It can be
seen from the simulation results that the temperature fluctuates
sinusoidally with time, the frequency of the temperature
change is basically consistent with the frequency of the vibra-
tion, and the magnitude of the temperature change increases as
the amplitude increases. When the amplitude is 1 mm, the

a) amplitude of 0.2 mm

b) vibration frequency of 10 Hz
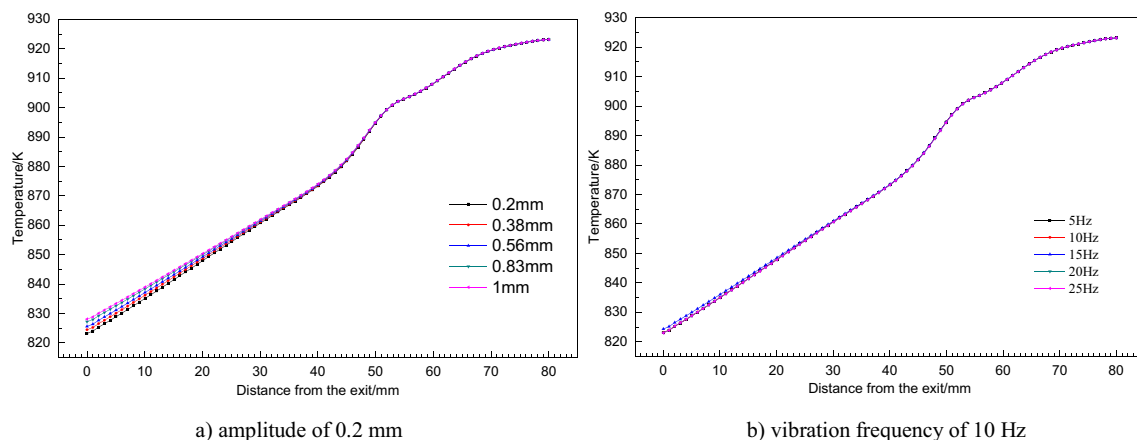
Fig. 11 Temperature distribution along the centerline of the molten pool under different vibration parameters. **a** Amplitude of 0.2 mm. **b** Vibration
frequency of 10 Hz
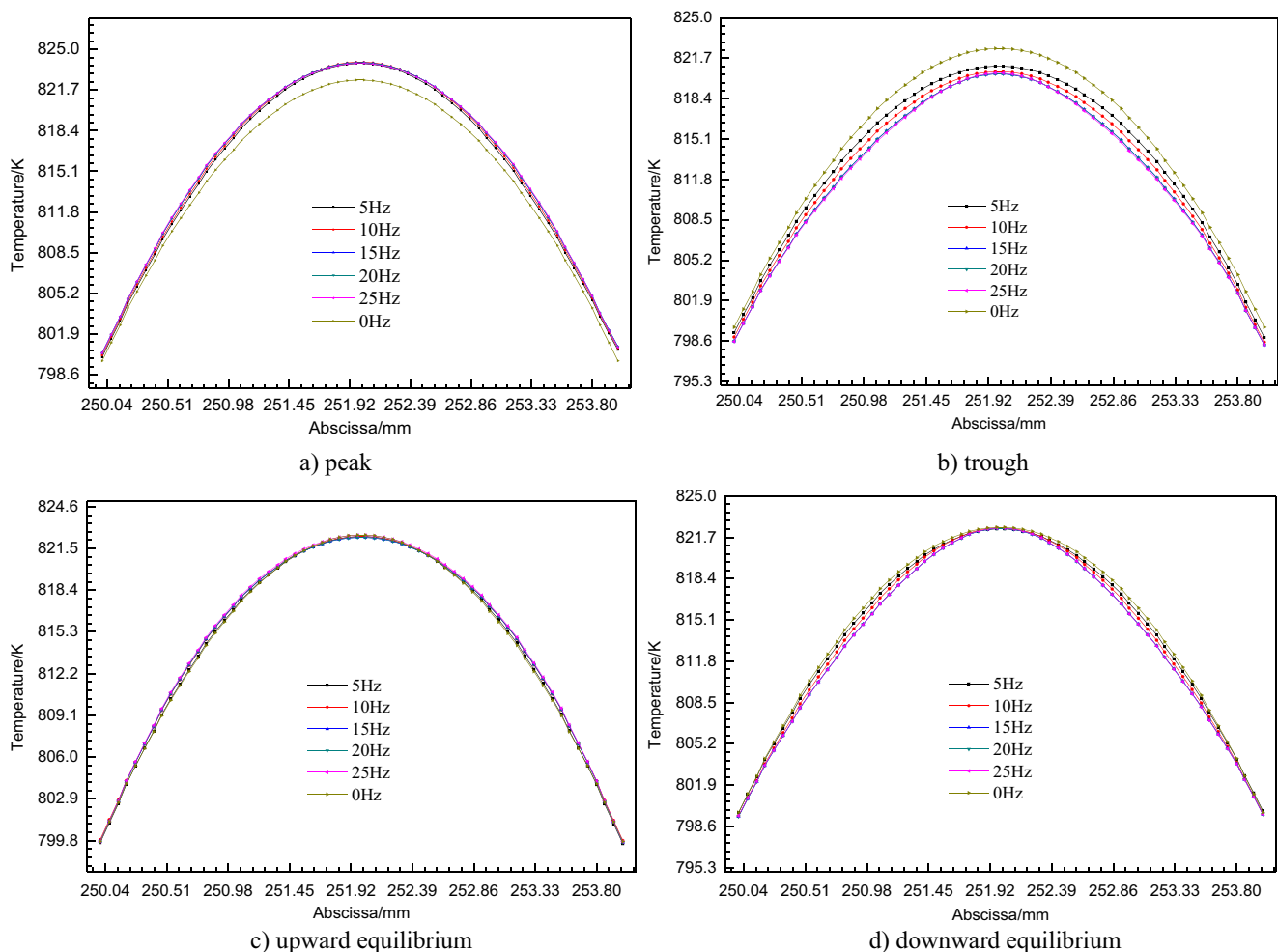
Fig. 12 Temperature distribution at the rolling exit at different vibration frequencies in each vibration phase. **a** Peak, **b** trough, **c** upward equilibrium, and **d** downward equilibrium

temperature change magnitude reaches a maximum of 23 K. It can also be observed that the average temperature decreases slightly with increasing amplitude. The average temperature at an amplitude of 1 mm is approximately 5 K lower than that for an amplitude of 0.2 mm. However, the vibration frequency has no effect on the average temperature. Compared with the phase of the vibration, the temperature change is relatively delayed as a whole, and the increase in the amplitude makes the phase delay very obvious.

5.1.2 Time-domain characteristics of the kiss point height

The kiss point height is an important parameter for the cast-rolling process. An overly high kiss point leads to an excessive rolling force, an increased cracking tendency of the strip, and even a "roll jamming" phenomenon, resulting in an interruption in the production. On the other hand, an insufficient kiss point height leads to a reduction in the plastic deformation zone, the formation of

shrinkage porosity and cavities, and even leakage of the molten metal. The above analysis of the temperature at the rolling exit shows that the vibration makes the temperature change periodically, so it can be inferred that the kiss point height would fluctuate along with it as well. The change in the kiss point height under different vibration parameters was obtained by simulation (as shown in Figs. 9 and 10) and can provide a reference for the determination of the optimal process parameters for vibration cast-rolling.

It can be seen in the Figs. 9 and 10 that the variation in the height of the kiss point under different vibration parameters is basically consistent with that of the temperature at the center of the rolling exit. The maximum magnitude of the height change is 10 mm, and the minimum value is 2.5 mm. However, since the change in the height of the kiss point causes the rolling force to fluctuate, thereby affecting the stability of the quality of the strip, it should not be too intense.
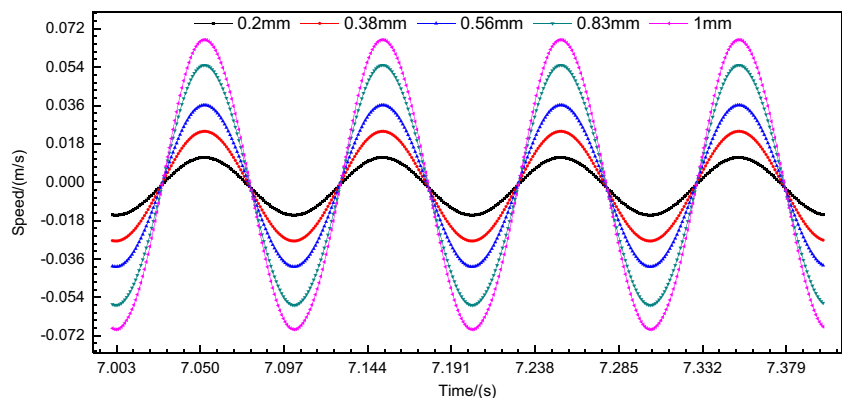
a) peak

b) trough

c) upward equilibrium

d) downward equilibrium
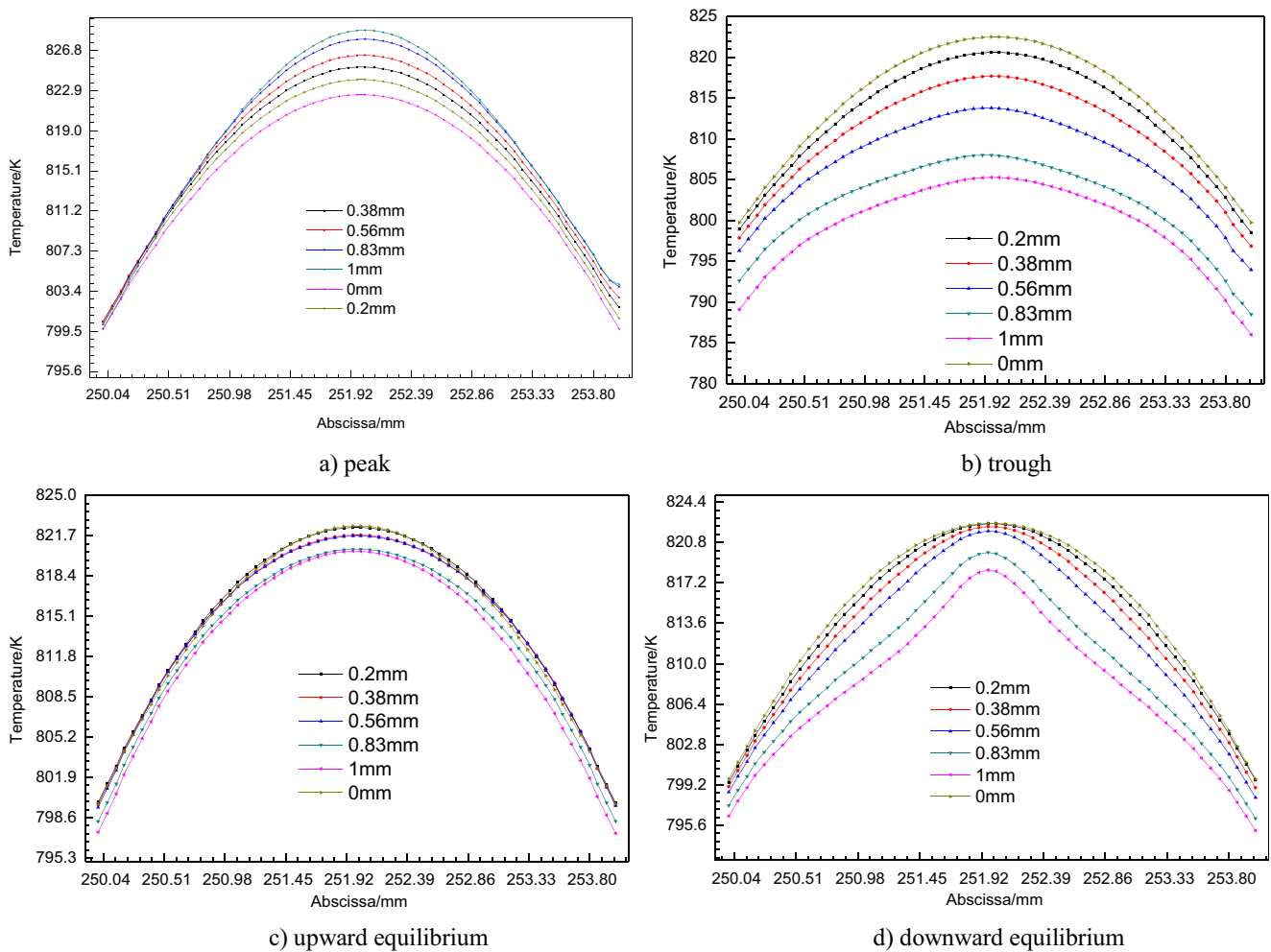
Fig. 13 Temperature distribution at the rolling exit at different amplitudes in each vibration phase. **a** Peak, **b** trough, **c** upward equilibrium, and **d** downward equilibrium

5.1.3 Effect of the vibration on the temperature distribution at the centerline of the molten pool
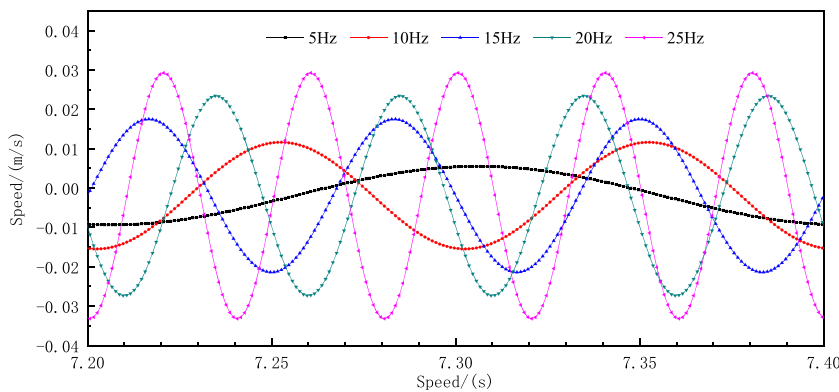
Figure 11 shows the temperature distribution along the centerline of the molten pool when the vibration phase is at the crest for different vibration parameters. It can be seen from the figure that the effect of the vibration along the centerline of the molten pool is much more obvious at the rolling exit than the center and upper part of the molten pool, indicating that the vibration mainly affects the heat transfer in the region with a high solid fraction and has little effect on the liquid phase.

Fig. 14 The history of the Y-direction velocity at the midpoint of the molten pool centerline at different amplitudes when the vibration frequency is 10 Hz

Fig. 15 The history of the *Y*-direction velocity at the midpoint of the molten pool centerline at different frequencies when the amplitude is 0.2 mm

Fig. 16 The history of the *X*-direction velocity at the midpoint of the molten pool centerline at different amplitudes when the vibration frequency is 10 Hz
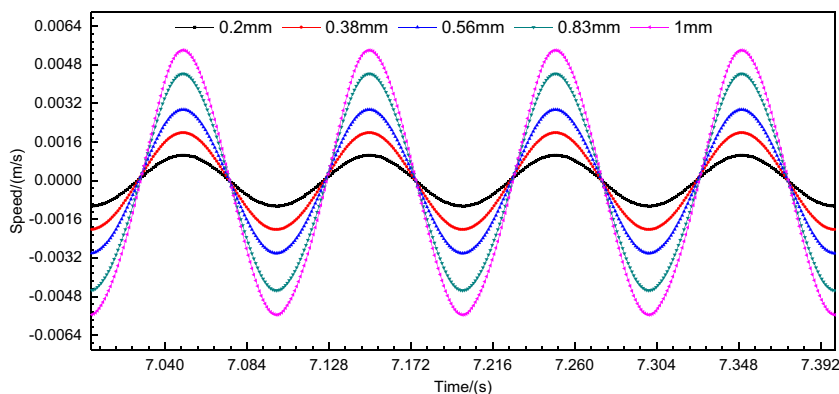
### 5.1.4 Effect of vibration on temperature distribution at the rolling exit

Since the temperature at the rolling exit varies periodically with the roll vibration, it is necessary to observe the temperature distribution at the rolling exit while the vibrating roll is located at four special vibration phases, such as upward equilibrium position, peak, downward equilibrium position, and trough, to explore the influence of the vibration parameters on the temperature distribution at the rolling exit.

Figure 12 shows the temperature distribution at the rolling exit for different vibration frequencies when the vibrating roll is in the four special vibration phases. The temperature is substantially symmetrically distributed, and the edge temperature is lower than the core temperature, which can be attributed to the very intense heat exchange between the edges and the rolls. It can also be found that the vibration frequency has little effect on the temperature distribution at the rolling exit.

Figure 13 shows the temperature distribution at the rolling exit for different amplitudes when the vibrating roll is in the four special vibration phases. It can be seen from the figure that the amplitude has a great influence on the temperature distribution on the strip at the rolling exit. Except for the peak phase, the vibration can effectively reduce the temperature of the strip at the rolling exit and reduce the temperature

Fig. 17 The history of the *X*-direction velocity at the midpoint of the molten pool centerline at different frequencies when the amplitude is 0.2 mm

a) nonvibration b) peak c) downward equilibrium d) trough e) upward equilibrium
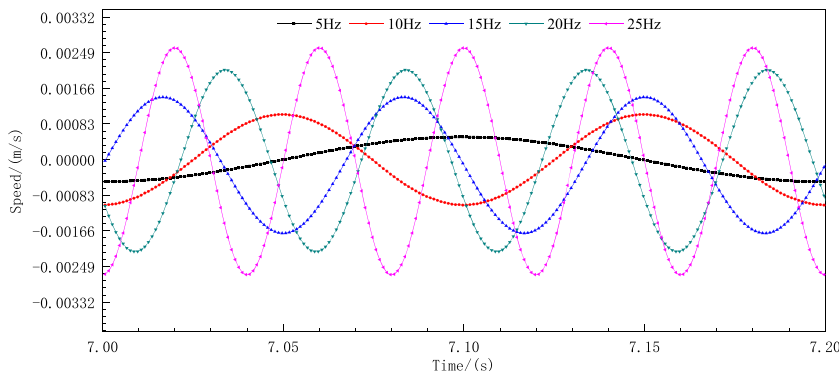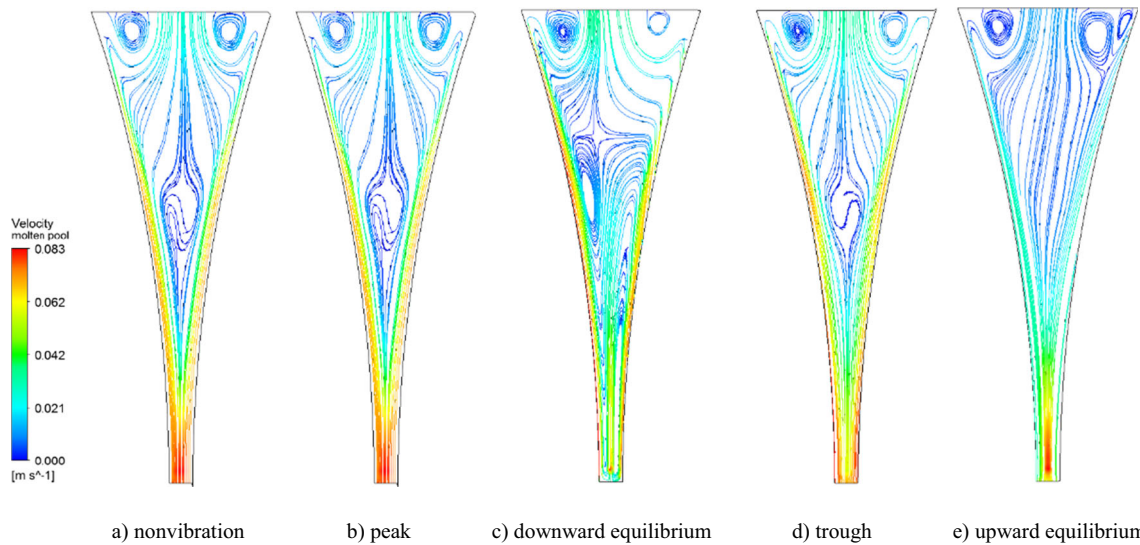
Fig. 18 Streamlines in the nonvibration and vibration cast-rolling molten pool when the vibration frequency is 10 Hz and the amplitude is 0.38 mm. **a** Nonvibration, **b** peak, **c** downward equilibrium, **d** trough, and **e** upward equilibrium

difference between the core and the sides to a certain extent. At the same time, the vibration also causes a slight shift of the temperature center because the vibration changes the contact state of the relatively high solid fraction with the roll surface, thereby affecting the heat exchange.

### 5.2 Effect of the vibration on the flow field

5.2.1 Time-domain characteristics of the flow field

Figure 14 shows the history of the Y-direction velocity at the midpoint of the molten pool centerline at different amplitudes when the vibration frequency is 10 Hz. The variation law is in line with the sinusoidal curve, which is similar to the shape of the motion curve of the vibrating roll; however, the speed change lags by 3/4 of a cycle in time compared with that of the roll motion. The velocity at the centerline of the molten

pool can reflect the flow state of the metal at the center of the molten pool, indirectly characterizing the intensity of the disturbance effect of the vibration on the molten pool. It can be seen from the figure that the peak value of the velocity increases as the amplitude increases.

Figure 15 shows the history of the Y-direction velocity at the midpoint of the molten pool centerline at different frequencies when the amplitude is 0.2 mm. As seen from the figure, the vibration frequency of the vibrating roll can affect the frequency and amplitude of the velocity variation at the same time. The greater the vibration frequency, the greater the frequency and amplitude of the velocity variation.

Figures 16 and 17 respectively show the influence of the amplitude and vibration frequency on the history of the X-direction velocity at the midpoint of the molten pool centerline, and the trend is basically consistent with that of the Y-direction velocity.

a) vibration frequency varies
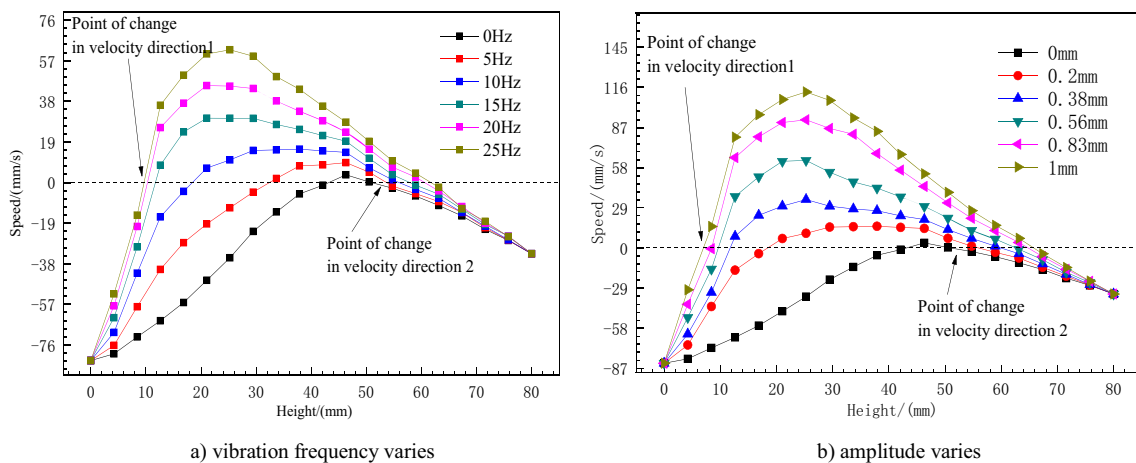
b) amplitude varies

Fig. 19 Y-direction velocity distribution along the centerline of the molten pool under different vibration parameters when the vibrating roll is at the downward equilibrium vibration phase. **a** Vibration frequency varies. **b** Amplitude varies
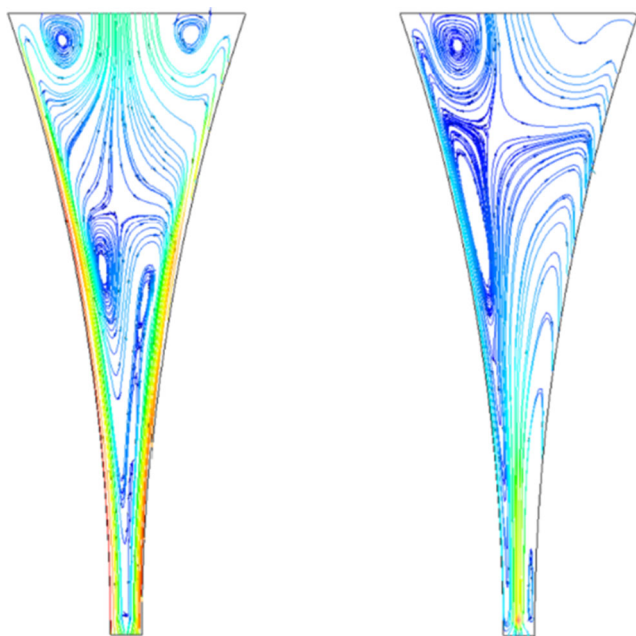
a) amplitude is 0.2 mm   b) amplitude is 1 mm

Fig. 20 Streamline distribution at the downward equilibrium vibration phase with different amplitudes when the vibration frequency is 10 Hz. **a** Amplitude is 0.2 mm. **b** Amplitude is 1 mm

5.2.2 Effect of the vibration on the velocity at the centerline of the molten pool

The flow field in the molten pool is mainly affected by the cast-rolling speed and the vibration of the roll. Figure 18 shows the streamlines in the nonvibration and vibration cast-rolling molten pools. The streamlines in the nonvibration molten pool are basically symmetrically distributed, and there is a large eddy in the core.

For vibration cast-rolling, when the vibrating roll is in the downward equilibrium position, a large eddy appears on the nonvibration side of the molten pool, where the molten metal flows in a clockwise direction, and the eddy can affect the rolling exit. On the vibration side of the molten pool, there is also an eddy, but the metal there flows counterclockwise. When the roll is at the peak and trough position, the flosw field of the molten pool is mainly affected by the cast-rolling speed because the vibration speed of the roll is zero, and the flow field is basically consistent with the nonvibrating flow field. When the roll is in the upward equilibrium position, the eddy in the core is dispersed under the combined action of roll rotation and vibration.

Velocity comparison at the centerline of the downward equilibrium position It can be seen from the above analysis that when the roll is at the peak or trough positions, the flow field of the molten pool is substantially identical to the nonvibrating flow field and changes greatly at the equilibrium positions. Therefore, it is necessary to study the influence of the vibration parameters on the velocity distribution along the centerline of the molten pool when the rolls are in the equilibrium position.

Figure 19a shows the distribution of the velocity in the Y-direction on the centerline of the molten pool under different vibration parameters when the vibrating roll is at the downward equilibrium position. The rolling direction is set as the negative direction, and the zero point of the speed indicates the direction change of the fluid velocity.

According to Fig. 19, the influence of the vibration frequency and amplitude on the velocity change in the Y-direction is similar. The velocity in the Y-direction on the centerline of the molten pool increases first and then decreases with decreasing position. There are two transitions in the direction, and there is a peak in the speed between the two transitions, and the speed returns to the cast-rolling speed at the rolling exit. As the frequency or amplitude increases, the distance between the two transition points for the velocity directions increases, and the peak point also moves toward the rolling exit. This change is due to an increase in the eddy size as the
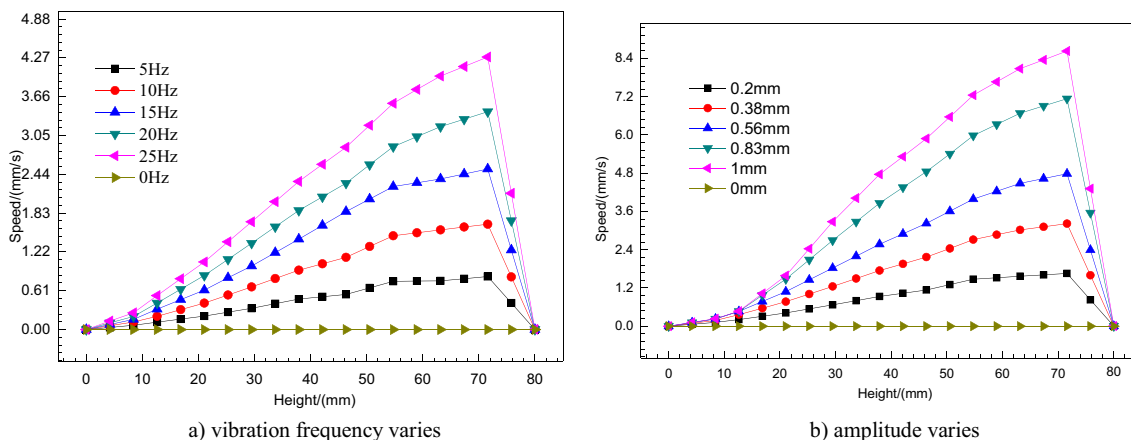
a) vibration frequency varies   b) amplitude varies

Fig. 21 X-direction velocity distribution on the centerline of the molten pool under different vibration parameters when the vibrating roll is at the downward equilibrium vibration phase. **a** Vibration frequency varies. **b** Amplitude varies

a) vibration frequency varies
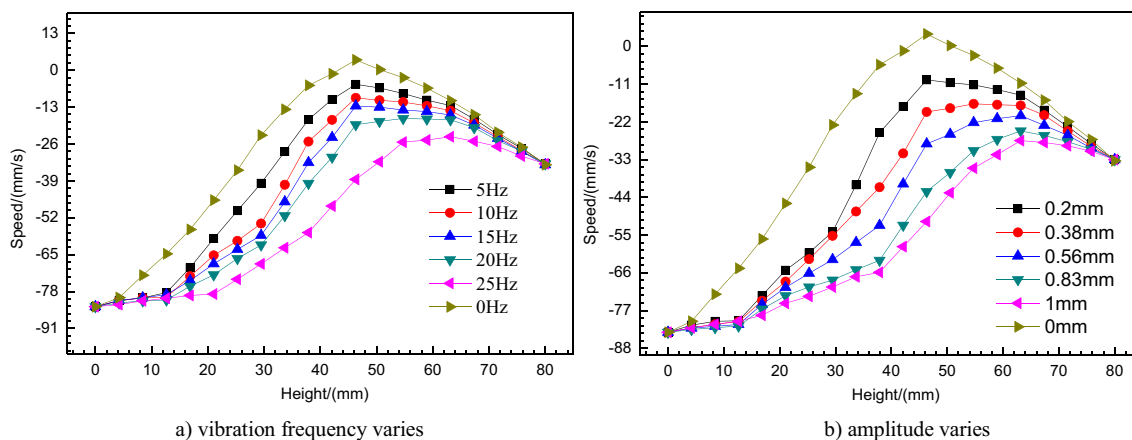
b) amplitude varies

Fig. 22 *Y*-direction velocity distribution on the centerline of the molten pool under different vibration parameters when the vibrating roll is at the upward equilibrium vibration phase. **a** Vibration frequency varies. **b** Amplitude varies

vibration amplitude increases (as shown in Fig. 20). The study by Lv et al. showed that the central segregation during cast-rolling is mainly due to an enrichment of the alloying elements at the kiss point under the action of the flow field. The vibration-induced eddy expands with an increase in the vibration intensity, and the disturbance effect at the kiss point is elevated, thereby enhancing the suppression effect on the element enrichment there and thereby effectively improving the center segregation defect in the cast-rolled strip.
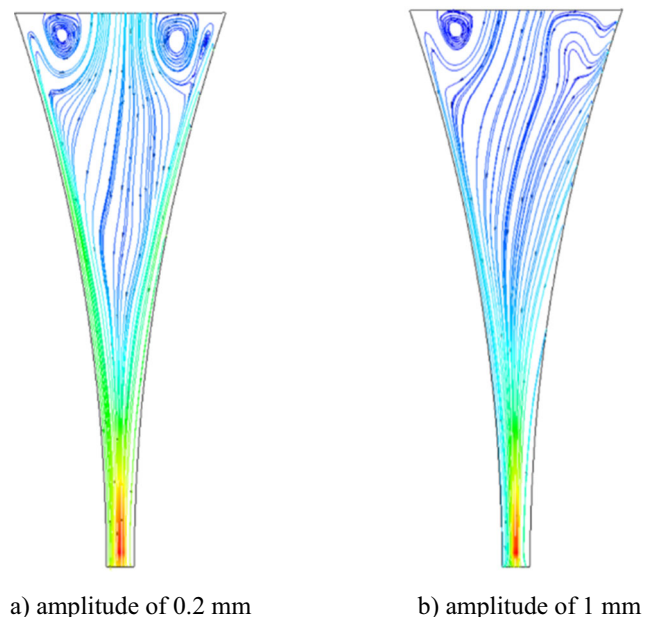
As shown in Fig. 21, the influence of the vibration frequency and amplitude on the velocity change in the *X*-direction is similar. The velocity in the *X*-direction on the centerline of the molten pool first increases and then decreases as the position gradually decreases. However, the direction of the velocity does not change, and the peak value of the velocity appears

a) amplitude of 0.2 mm   b) amplitude of 1 mm

Fig. 23 Streamline distribution at the upward equilibrium vibration phase with different amplitudes when the vibration frequency is 10 Hz. **a** Amplitude of 0.2 mm. **b** Amplitude of 1 mm

in the upper part of the molten pool. This phenomenon is caused by the vibration-side eddy gradually expanding with increasing vibration intensity and squeezing the nonvibration-side eddy, causing the flow field distribution in the molten pool to tilt toward the nonvibration side. It can also be seen from the figure that the amplitude has a slightly greater influence on the velocity distribution on the centerline of the molten pool than the vibration frequency.

Velocity comparison at the centerline of the upward equilibrium position Figure 22 shows the distribution of the velocity in the *Y*-direction along the centerline of the molten pool when the vibrating roll is in the upward equilibrium position under different vibration parameters. Since the vibrating roll is moving in the opposite direction to the rolling direction at this time, the backflow is reduced. Therefore, the *Y*-direction speed of the metal on the centerline is downward, and the absolute value of the velocity increases as the amplitude increases.

It can be seen in Fig. 23 that an eddy appears on both sides of the nozzle when the vibrating roll is in the upward equilibrium position. The increase in the vibration intensity causes the vibration-side eddy to expand and press the nonvibration-side eddy, causing the metal flow line to tilt toward the nonvibration side.

Figure 24 shows the distribution of the velocity in the *X*-direction along the centerline of the molten pool when the vibrating roll is in the upward equilibrium position under different vibration parameters. The distribution trend is similar to that when the vibrating roll is at the downward equilibrium vibration phase.

5.3 Determination of the optimal vibration parameters

It would be ideal for the vibration to strongly disturb the flow field in the molten pool during twin-roll strip vibration cast-

a) vibration frequency varies   b) amplitude varies
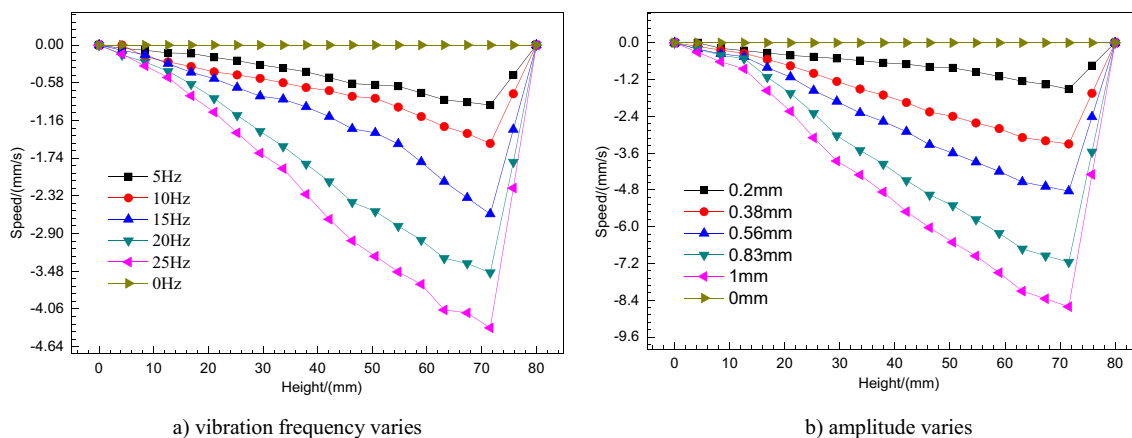
Fig. 24 *X*-direction velocity distribution on the centerline of the molten pool under different vibration parameters when the vibrating roll is at the upward equilibrium vibration phase. **a** Vibration frequency varies. **b** Amplitude varies

a) fluctuation amplitude   b) average value
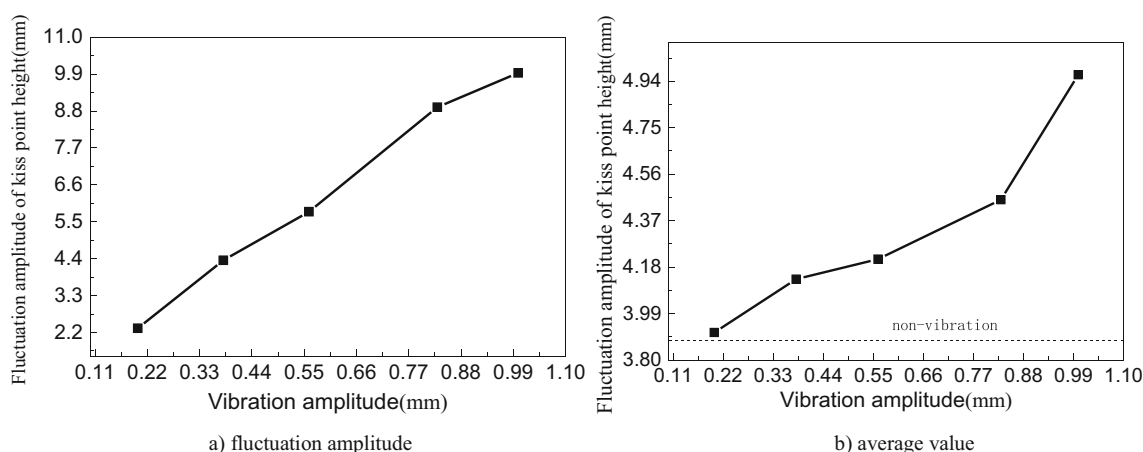
Fig. 25 The variation lows of the fluctuation amplitude of and average value of the kiss point height with the increase of vibration amplitude when the vibration frequency is 10 Hz. **a** Fluctuation amplitude. **b** Average value

rolling and thereby refine the grains and suppress segregation. At the same time, this disturbance does not make the fluctuation of the kiss point height too intense, so it does not affect the stability of the process.

According to the previous analysis, the vibration amplitude determines the fluctuation amplitude of the kiss point height, and the vibration frequency only changes the fluctuation frequency. It can be seen from Fig. 25a that under the condition that the amplitude takes a maximum value of 1 mm, the kiss point is always kept above the rolling exit, so liquid leakage does not occur. However, to ensure the stability of the vibration cast-rolling process, it is still necessary to control the

fluctuation amplitude of the kiss point height within a reasonable range. It can be seen from Fig. 25b that the average value of the kiss point height increases with increasing vibration amplitude, but the increase is not significant over the amplitude range of 0.38 mm to 0.56 mm, and the rate of the increase is significantly improved after the amplitude exceeds 0.56 mm. Therefore, to ensure the stability of the cast-rolling process from the perspective of the kiss fluctuation, the vibration amplitude should be controlled below 0.56 mm.

On the other hand, if the acceleration of the roll vibrating downward is greater than the gravitational acceleration, there is a possibility that blanking occurs, which not only affects the heat exchange of the vibration-side roller surface but also may cause side leakage of the molten pool in the worst case. Therefore, the vibration parameters of the cast-rolling must satisfy $A(2\pi f)^2 \leq 9800$, where A is the amplitude (mm) and f is the vibration frequency (Hz). According to this requirement, the limiting vibration frequencies corresponding to different amplitudes are shown in Table 6.

Table 6 Limit frequencies corresponding to different adjustable amplitudes

Number	1	2	3	4	6
Amplitude	0.2 mm	0.38 mm	0.56 mm	0.83 mm	1 mm
Limit frequency	25 Hz	25 Hz	20 Hz	17 Hz	15 Hz

Fig. 26 Velocity at the midpoint of the molten pool centerline under the two sets of candidate optimal vibration parameters
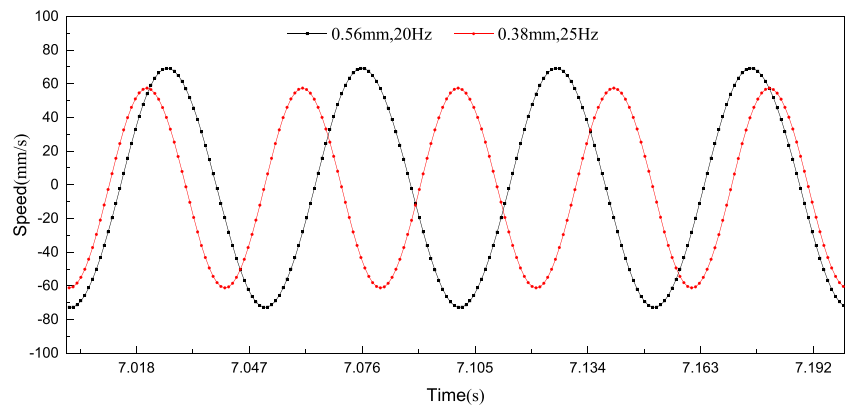
When the amplitude is 0.2 mm, the calculated limiting vibration frequency is greater than the maximum vibration frequency that can be adjusted on the vibration cast-rolling mill, that is, 25 Hz, so the actual limit vibration frequency is 25 Hz.

According to the above analysis, both a vibration frequency and an amplitude increase mean an increase in the vibration intensity, which also means an increase in the disturbance effect of the vibration on the molten pool. Therefore, two sets of vibration parameters in Table 6, such as the parameters in the second group and the third group, are selected as the candidate optimal vibration parameters. Figure 26 shows the velocity at the midpoint of the molten pool centerline under the two sets of vibration parameters. In comparison, it can be found that under the third group of vibration parameters, the vibration has a stronger disturbance effect on the molten pool than under the second group of vibration parameters. Therefore, the optimal vibration parameters of the 7075 aluminum alloy vibration cast-rolling process are determined to be an amplitude of 0.56 mm and vibration frequency of 20 Hz.

6 Conclusion

1. The results of the vibration cast-rolling experiment of the 7075 aluminum alloy show that the vibration can effectively refine the grains and inhibit segregation, thus improving the mechanical properties.
2. A thermal-flow-coupled numerical simulation model of vibration cast-rolling considering solidification is established herein, and the accuracy of the model is verified by the collected strip temperature. Then, the model is used to further analyze the time-domain characteristics of the temperature field, flow field, and kiss point position in the molten pool of vibration cast-rolling. The results show that the amplitude has a great influence on the kiss point fluctuation, and both the amplitude and vibration frequency can obviously disturb the flow field in the molten pool.

3. The disturbance of the vibration on the flow field in the molten pool is the main factor for refining the grains and suppressing the segregation of alloying elements.
4. The optimal vibration parameters for the 7075 aluminum alloy vibration cast-rolling process are determined to be an amplitude of 0.56 mm and a frequency of 20 Hz.

References

1. Sahoo S, Kumar A, Dhindaw BK, Ghosh S (2012) Modeling and experimental validation of rapid cooling and solidification during high-speed twin-roll strip casting of Al-33 wt pct Cu. Metall Mater Trans B Process Metall Mater Process Sci 43(4):915–924
2. Pelss A, Rückert A, Pfeifer H (2015) Physical simulation of the flow field in a vertical twin roll strip caster-a water model study. Steel Res Int 86(7):716–723
3. Parsunkin BN, Andreev SM, Logunova OS, Akhmetov TU (2015) Energy-saving optimal control over heating of continuous cast billets. Int J Adv Manuf Technol 79(9-12):1797–1803
4. Rodrigues C, Ludwig A, Kharicha A, Wu M (2018) Modeling of the twin-roll casting process: transition from casting to rolling. Trans Indian Inst Metals 71(11):2645–2649
5. Li JT, Xu GM, Yu HL, Deng GY, Su LH, Lu C, Li HJ (2015) Optimization of process parameters in twin-roll strip casting of an AZ61 alloy by experiments and simulations. Int J Adv Manuf Technol 76(9-12):1769–1781
6. Zhang N, Tang P, Zhu MM, Wen G, Ma F (2010) Research metal delivery system of twin-roll thin strip continuous caster for magnesium alloys. Mater Rev 24(16):237–240
7. Miao YC, Zhang XM, Di HS, Wang GD (2006) Numerical simulation of the fluid flow, heat transfer, and solidification of twin-roll strip casting. J Mater Process Technol 174(1-3):7–13
8. Bae JW, Kang CG, Kang SB (2007) Mathematical model for the twin roll type strip continuous casting of magnesium alloy considering thermal flow phenomena. J Mater Process Technol 191(1-3):251–255
9. Zhang XM, Jiang ZY, Liu XH (2006) Simulation of fluid flow, heat transfer and micro-segregation in twin-roll strip casting of stainless steel. J Mater Sci Technol 22(3):295–300

10. Zhang XM, Jiang ZY, Yang LM, Liu XH, Wang GD, Tieu AK (2007) Modelling of coupling flow and temperature fields in molten pool during twin-roll strip casting process. J Mater Process Technol 187:339–343

11. Lv Z, Du F, An Z, Huang H, Xu Z, Sun J (2015) Centerline segregation mechanism of twin-roll cast A3003 strip. J Alloys Compd 643:270–274

12. Chang LL, Cho JH, Kang SK (2012) Microstructure and mechanical properties of twin roll cast AM31 magnesium alloy sheet processed by differential speed rolling. Mater Des 34:746–752

13. Gras C, Meredith M, Hunt JD (2005) Microdefects formation during the twin-roll casting of Al-Mg-Mn aluminium alloys. J Mater Process Technol 167(1):62–72

14. Xu ZQ, Meng ZR, Xue SH, Zhang DQ, Du FS (2018) Effect of oscillation parameters to flow field in the pool during the oscillating twin-roll strip casting process. Chin J Mech Eng 31(1):1–8

15. Du FS, Sun MH, Huang SG, Wei JP, Huang HG, Xu ZQ (2018) Mechanism and simulation experiments on twin-roll thin-strip vibration casting. China Mech Eng 29(4):477–484

16. Wei JP, Xu ZQ, Sun MH, Zhu ZW, Wang HJ, Du FS (2018) Experimental research of vibratory cast-rolling strips for 20crmn alloy steel. Ironmak Steelmak 53(12):118–121